The Relationship between Backward Compatible Assembly and Microstructure on the Thermal Fatigue Reliability of an Extremely Large Ball Grid Array

Richard Coyle, Richard Popowich, Peter Read, and Debra Fleming Alcatel-Lucent, Murray Hill, NJ
Raiyo Aspandiar, Alan Donaldson, and Vasu Vasudevan, Intel, Corporation, Hillsboro, OR
Iulia Muntele, Sanmina-SCI Corporation, Huntsville, AL
Stephen Tisdale, Intel, Corporation, Chandler, AZ
Robert Kinyanjui, formerly of Sanmina-SCI Corporation, Huntsville, AL

ABSTRACT
Accelerated temperature cycling was used to evaluate the thermal fatigue reliability for the case of backward compatible assembly (mixed alloy, Pb-free BGA/SnPb paste) of a 3162 pin count, extremely large body (51.0 mm x 59.5 mm) ball grid array (BGA). The BGA component was fabricated with Sn-4.0Ag-0.5Cu (SAC 405) Pb-free solder balls and surface mount assembly was done using SnPb eutectic soldering profiles. The profiles were selected to simulate situations involving incomplete mixing in order to study the effect of various levels of Pb mixing and microstructure on solder joint quality and thermal fatigue reliability. Although the most common criteria for acceptable mixed alloy assembly are uniform or 100% Pb mixing throughout the solder joint and complete ball collapse during reflow, these criteria can be difficult to meet with larger BGA packages due to thermal issues. The effect of such imperfect mixing on reliability of large packages is unknown. The test program included Pb-free, SAC405 assemblies to provide a reliability baseline comparison. Testing was done using a 0 to 100 °C temperature cycle with 10 minute ramp and dwell times and post-cycling failure analysis was conducted on representative test samples. Baseline characterization and failure analysis included optical metallography and scanning electron microscopy (SEM). The thermal cycling test data and failure analysis results are discussed in terms of the relationship to the initial as well as evolving Pb-free and mixed alloy microstructures. The reliability data indicate that mixed assemblies can provide acceptable reliability, even in some cases when Pb mixing is not complete or uniform. However, these results also show that warpage effects can increase the operating risk by reducing the process margin. Further, it is shown also that the reliability likely is influenced more by the underlying Pb-free microstructure than by the Pb introduced by mixed assembly.

INTRODUCTION
Most high reliability electronic equipment producers continue to manufacture and support tin-lead (SnPb) electronic products despite the increasing trend for design and conversion to Pb-free manufacturing. These equipment suppliers can continue to use SnPb solder assembly and remain in compliance with the RoHS Directive (restriction on certain hazardous substances) by invoking the European Union Pb-in-solder exemption [1]. At the same time, companies are facing increased pressure from a component supply chain that is rapidly converting to Pb-free offerings and thus has a decreasing motivation to continue producing SnPb product for these low-volume end users [2]. Until recently these supply chain constraints were limited to high volume, small ball grid array (BGA) packages components such as memory devices. Now there is a growing concern surrounding availability of larger SnPb BGA components. For various reasons, complete Pb-free conversion is not always a viable option and consequently, these availability issues can force companies to use Pb-free BGAs with the SnPb solder assembly process. Pb-free BGAs with SnPb surface mount assembly, often referred to as backward compatible or mixed alloy processing, provides an alternative manufacturing path if immediate, complete product conversion to Pb-free manufacturing is not possible.

The technical issues associated with mixed alloy processing have been addressed in a significant number of studies [3-51] and those results have been reviewed and discussed in detail in previous publications [3, 48, 49, 50]. A review of the literature shows that most of those studies have been focused on the optimization of process parameters that produce acceptable solder joint quality. This is expected because mixed alloy assembly is not drop-in replacement process. Mixed alloy studies using smaller BGA devices have shown that acceptable thermal fatigue reliability can be achieved with backward compatible processes [3, 6, 49, 50]. However, there is a gap in the mixed alloy thermal fatigue reliability data for BGA packages with a body size greater than 35 mm. It is necessary to develop reliability data for larger packages because achieving acceptable mixed alloy assembly is extremely challenging as the package size and board complexity increases. The effect of large thermal mass and component warpage on Pb mixing was demonstrated by the work of Kinyanjui et al [48]. Therefore it is critical to understand the effect of imperfect mixing on reliability of large packages. In general, the literature indicates that there are fundamental inconsistencies and gaps that limit the understanding of mixed alloy reliability, particularly with larger body packages [4, 15, 16, 18, 32, and 35, 48, 49, 51].

This paper presents temperature cycling results for an extremely large body (51.0 mm x 59.5 mm), 3162 ball count, ball grid array (BGA) assembled using backward compatible, mixed alloy processing. The surface mount assembly profiles were designed to produce both complete and incomplete Pb mixing in the solder joints. The latter case simulates the condition of non-optimized mixed assembly to allow evaluation of the effects of incomplete Pb mixing and microstructure on solder joint quality and thermal fatigue reliability.

EXPERIMENTAL

Test Vehicle Design

The detailed package test vehicle attributes for the large-body BGA test vehicle are listed in Table 1. The populated printed circuit board test vehicle and the BGA pin diagram are shown in Figure 1. This is an 8 layer test board with dimensions 12 inches x 8 inches x 0.093 inches (305 mm x 203 mm x 2.36 mm). The board contains two different component footprints but only the larger one (51.0 mm x 59.5 mm, 3162 ball count) is used in this study. The test board contains component sites with either metal defined (MD) or soldermask defined land patterns (SMD) but only the sites with MD lands are used in this study. The MD lands are 17 mils in diameter and the surface finish on the test vehicle is organic solderability preservative (OSP). There is one daisy chain net for each land pattern. A number of lands on and near the corner areas as well as similar corner sites at the die shadow of the land patterns are not connected within the daisy chain. Typically these corner ball locations are not electrically functional on comparable product packages that use this design and are termed non critical to function (NCTF). Daisy chain nets from each of the components patterns are routed out to a card edge connector and soldered connections are used to monitor the resistances of the daisy chain nets during temperature cycling.

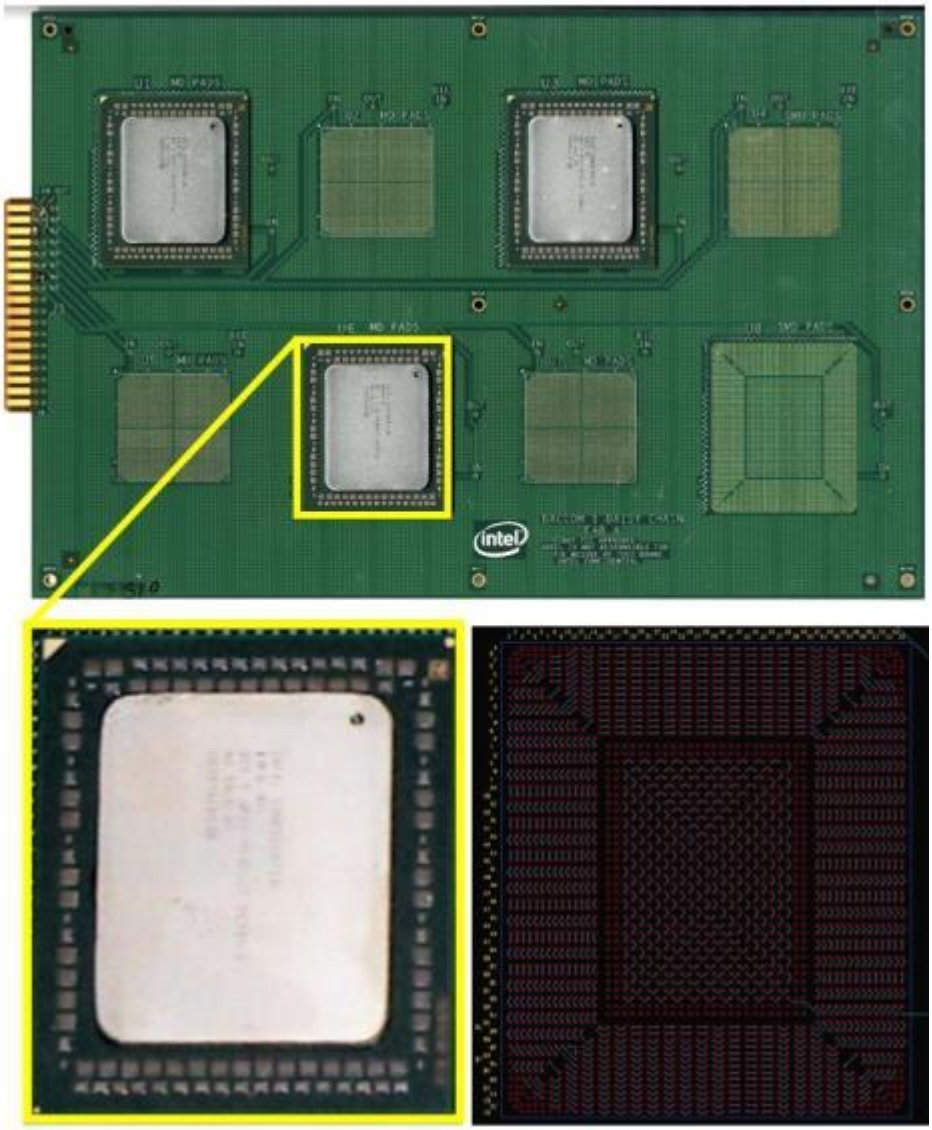

Figure 1: Populated daisy chained test board, top view of large body-BGA and BGA pin diagram.

Table 1: Package Test Vehicle Information

Test Vehicle Description	Package Attributes
Package Size	**51.0 x 59.5 mm**
Die size	**22.4 x 29.5 mm**
Substrate thickness	**1.500 mm**
Solder ball diameter	**0.508 mm**
Ball Pitch	**1.1016 mm**
Solder ball metallurgy	**SAC405**
Ball count	**3162**
Ball Pattern	**Fully populated grid with selective corner and die shadow depopulation**

Mixed Assembly Process Characterization

As mentioned above, the experimental strategy for this work entailed three legs, a partial Pb mixing leg, a full Pb mixing leg and a lead-free leg that acts as the control leg. A thermocouple board was prepared to develop the reflow profiles that can enable these levels of Pb mixing. The schematic of this thermocouple board is shown in Figure 2. Thermocouples were attached to all three BGA sites (U1, U3, and U6) populated with the package TV. Each package TV had five thermocouples attached, one at each of the four corners (TC1, TC2, TC3, and TC4) and one at the center (TC5). Each of these thermocouples had fine tips (diameter = 0.005 inches) and were placed at the center of solder joint by drilling from the bottom side of the test board. The direction of travel of the test board through the reflow oven is also shown in Figure 2.

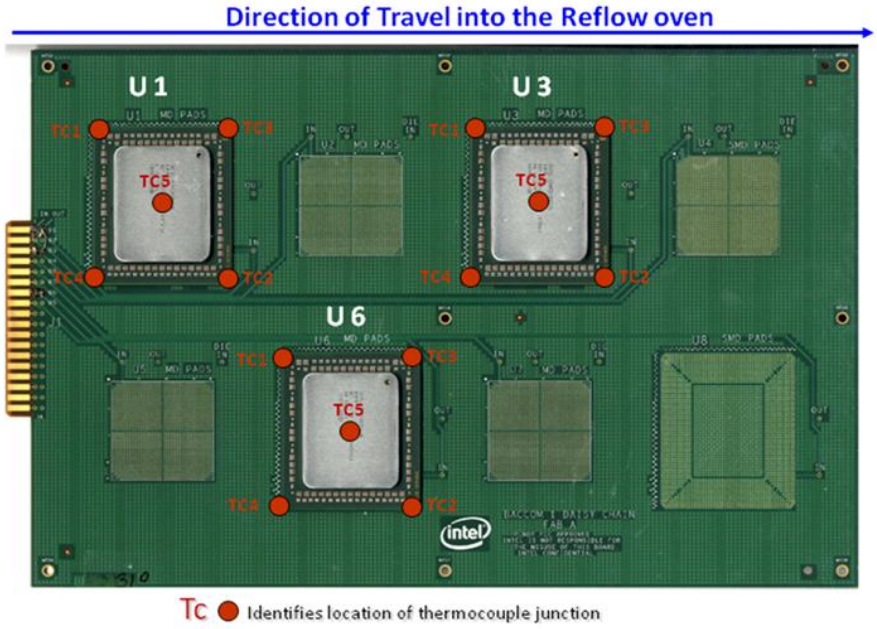

Figure 2: A schematic of the reflow profile development board showing the thermocouple locations.

A 0.006 inch thick laser-cut stencil with a circular opening, measuring 0.018 inches was used for solder paste printing. However, based on the known dynamic warpage performance of the BGA package TV, an increased amount of solder paste was required for the three outer peripheral rows to diminish the risk of the head-on-pillow (HoP) defect. Therefore, a 0.022 inch stencil opening was used for these rows only. A no-clean, Halogen-free, ROL0, near eutectic SnPb Type 4 solder paste was employed during the assembly of boards for Leg 1 and Leg 2. Similarly, a no-clean, ROL0, SAC305 composition Type 4 solder paste was used during the assembly of boards for Leg 3.

Figure 3 portrays the reflow profile window for each of the three legs of the designed experiment. The Leg 1 reflow profile window generated solder joints with partial mixing of Pb. The %Pb mixing levels in these solder joints varied from 23% to 86%. Multiple reflow profiling iterations were required to establish the reflow window of this leg. The initial reflow profile generated solder joints on the outside rows that were 100% mixed with Pb. To distinguish this Leg 1 from Leg 2, during subsequent reflow profile development, the temperature was lowered to reduce the %Pb mixing levels below 100%. It is obvious that the final Peak Reflow Temperature range is very wide, varying from 203 °C to 224 °C. This large window is necessary because of the large body size and high thermal mass of the BGA package test vehicle. However, it also is obvious

from Figure 3 that both the Leg 1 and Leg 2 reflow profile windows are outside the typical Sn-Pb eutectic soldering reflow window used in the industry.

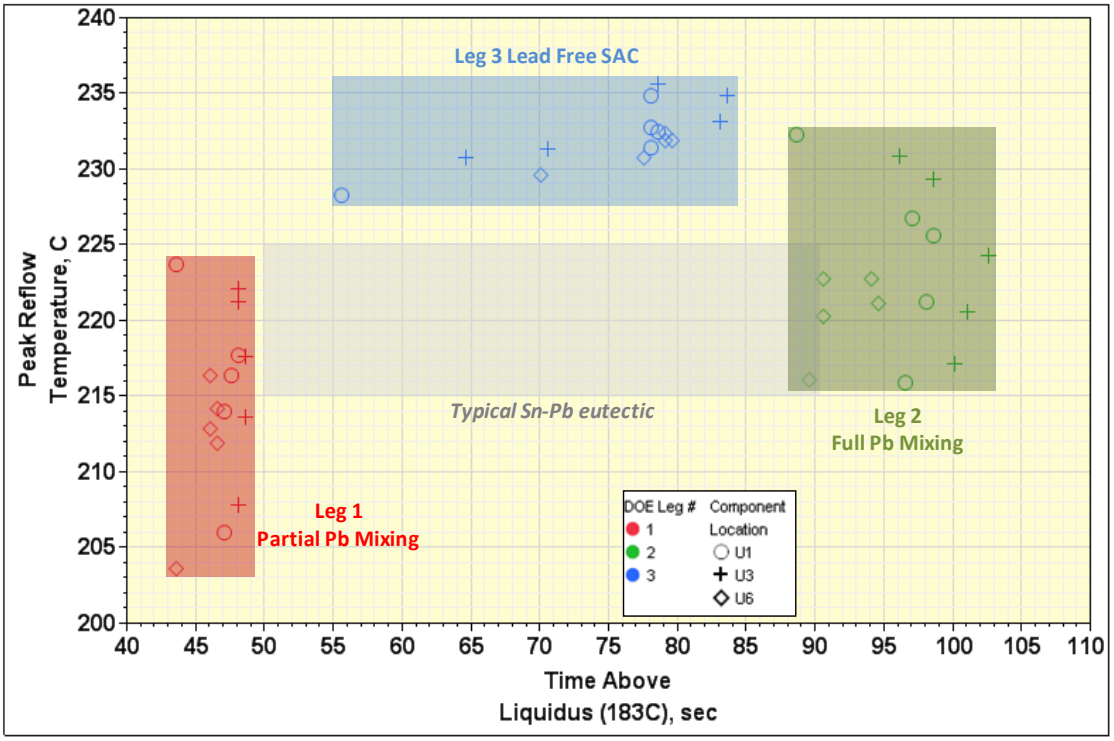

Figure 3: Reflow profile windows for the three Legs of the DOE using three package test vehicles on the test board

Backward compatibility solder joints are characterized by a so-called "mixed" microstructure [6-7, 48-50,]. As the Sn-Pb solder paste printed on the board land melts during reflow assembly, the Pb diffuses upwards within the lead-free SAC solder ball. Figure 4 shows an optical photomicrograph of a mixed BGA solder joint cross-section with partial or incomplete Pb mixing. The Pb mixed region is shown towards the printed circuit board side of the solder joint. For a fully mixed solder joint, the Pb mixed region would encompass the entire solder joint, right up to the package land.

The extent of Pb mixing can be quantified by measuring the height to which the Pb has diffused into the SAC solder ball and calculating this height as percentage of the solder joint height. Equation 1 gives the formula for % Pb mixing in the mixed alloy solder joint.

$$\% \text{ Pb Mixing} = 100*(H1-H2)/H1 \quad \text{.....(1)}$$

Figure 4 defines H1 and H2. H1 is the distance from the top of the package land to the top of the board land and is essentially the solder joint height or standoff. H2 height is calculated by measuring the distance from the top of the package land to the average height location of the Pb-mixed region.

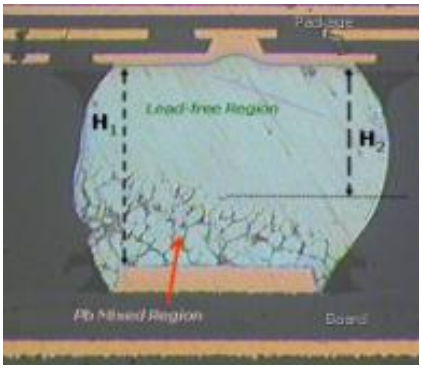

Figure 4: Photomicrograph of a partially mixed alloy solder joint illustrating the Pb mixing level calculation.

To determine the Pb mixing in the solder joints of the assembled board test vehicle, solder joints of the BGA package test vehicle assembled on all three locations (U1, U3, and U6) on the board test vehicle were cross-sectioned. Figure 5 indicates the locations of the three cross-section cuts on the ball map of the BGA package. These three cuts, which were performed on each assembled package on reflow profile validation boards, are identified as the a) outer row, b) the die shadow row, and c) the inner row in this figure. After polishing, specific solder joints in each cross-section, as indicated by the ball numbers in Figure 5, were inspected using an optical microscope and the %Pb mixing measured as explained in Figure 4.

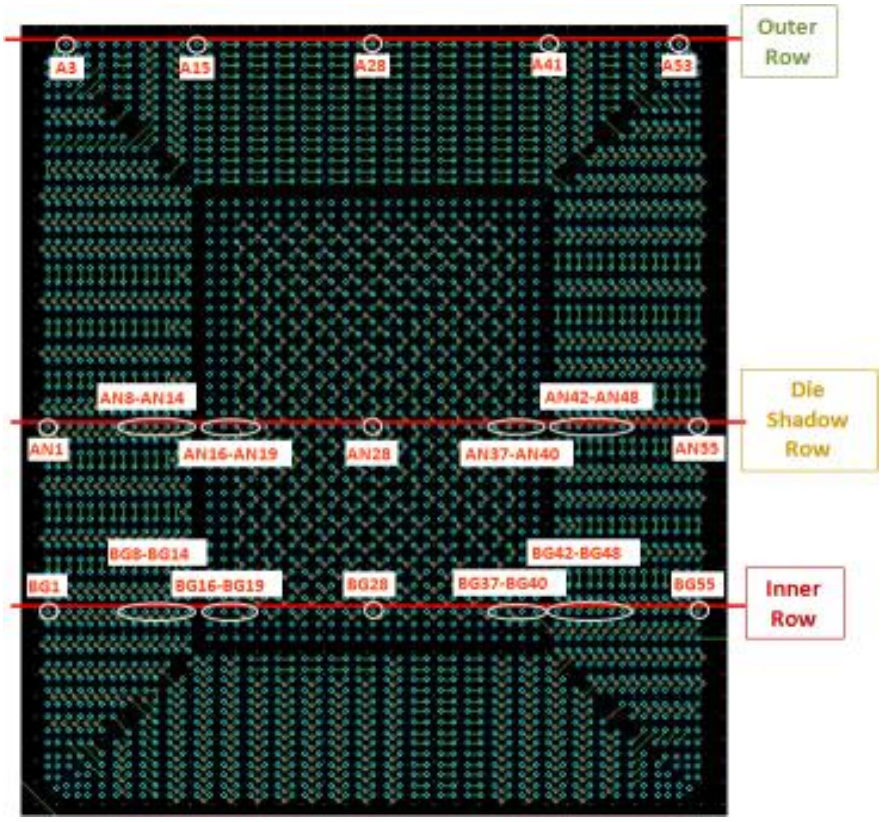

Figure 5: Ball map of the BGA package test vehicle showing the location of the three cross-section cuts as well as the ball numbers of the solder joints whose %Pb mixing levels were measured after polishing the cross-sections

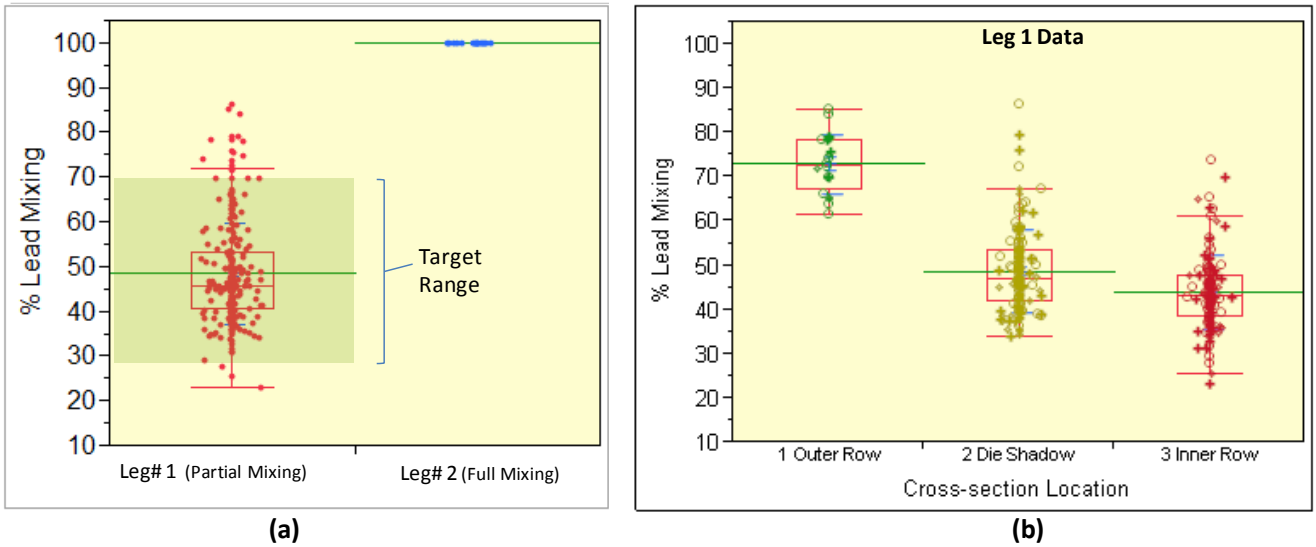

Figure 6: (a) Comparison of% Pb mixing in the solder joints for Leg 1 and Leg 2; (b) comparison of % Pb mixing in Leg 1 solder joints at outer row, die shadow row and inner row cross-section cut locations

The wide range in %Pb mixing in Leg 1 requires further investigation. Figure 6b shows the box plots for %Pb mixing in the solder joints with the location within the package where the cross-section cut was made. As is apparent in this figure from the box plots, the levels of %Pb mixing decrease and their range of values increases as the location of the cross-section cuts moves from the outer row towards the interior of the package, i.e., first the die shadow row and then the inner row. A closer look at the profile of the %Pb mixing values across these rows indicates the reason for these trends.

Figure 7 shows the variation in % Pb mixing within BGA solder joints that was measured across solder balls in three cross-section cuts made at various location on 6 package test vehicles which were assembled using Leg 1 reflow profile parameters. The upper plot is for the cross-section cut on the outer row, the middle plot is for the cross-section row on the die shadow row and the lower plot is for cross-section on the inner row. The locations of these three rows with respect to the ball map of the BGA package can be seen in Figure 5 above.

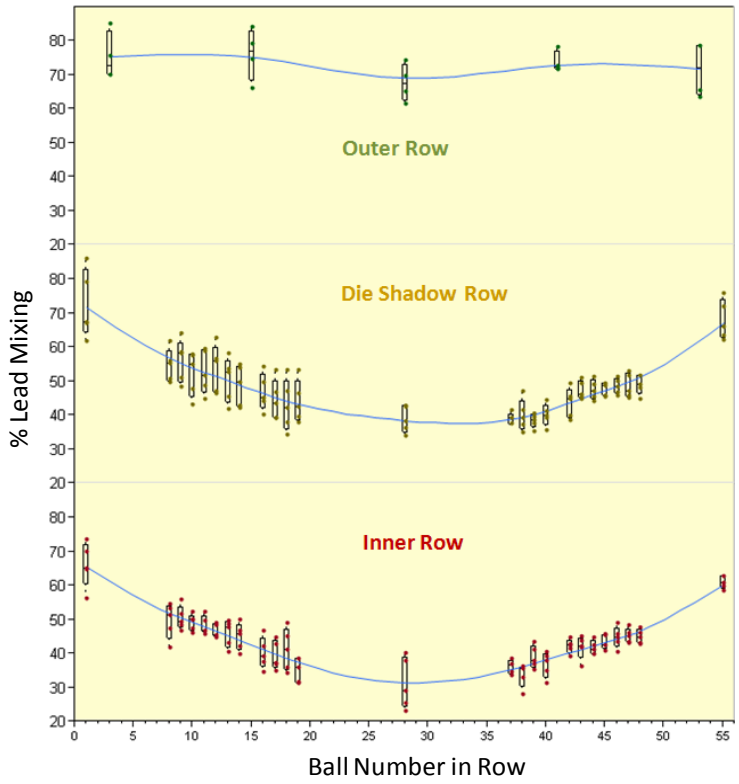

Figure 7: Plots showing the variation of the %Pb mixing in the BGA solder joints across the solder balls in the three cross-section cuts made at various locations on a total of six package test vehicles assembled for Leg 1.

Figure 7 clearly illustrates the wide variation in the %Pb mixing across the solder joints of the large BGA package test vehicle under evaluation. The outer row has a fairly uniform distribution of the %Pb mixing in the solder joints across its entire length. The die shadow row and inner row have, in contrast, a non-uniform distribution of the %Pb mixing across the solder joints in those rows. The solder joints in the middle of the rows, those that are under the die or close to the central location of the package body, have a significantly lower %Pb mixing (in the 25-50% range) than those on the edges of the rows, close to the edge of the package body. As expected, the %Pb mixing levels in the inner row towards the central part of the package are slightly lower than those in the die shadow row.

This wide variation in the %Pb mixing is a direct result of the temperature gradient across the solder joints under the large package body. The solder joints in the central part of the package do not get to as high a peak reflow temperature and are above the solder liquidus temperature for much shorter duration than those at or near the edges of the packages on the outer rows. Since the Pb diffusion from the molten Sn-Pb solder paste on the lands into the still solid SnAgCu solder ball is directly proportional exponentially to the temperature and linearly to the time, the solder joints that reach a lower peak temperature for a shorter time above liquidus will exhibit a lower %Pb mixing within them.

These results illustrate the difficulty in attaining uniform %Pb mixing levels across the entire array of mixed alloy solder joints for larger BGA components, for convection reflow soldering processes.

Solder Joint Stand-off Height

Solder joint stand-off height is critical to thermal fatigue reliability. Taller BGA solder joints are expected to be more reliable. Solder joint stand-off heights of large body BGA packages differ significantly across its ball array pattern after its assembly on the board. Therefore it was imperative to characterize this stand-off height variation across the assembled package for all three legs of the experiment.

Figure 8a shows box plots of the solder joint heights for all three legs. For Leg 1, stand-off height data was collected for three packages on two boards, for a total of 6 packages. For Leg 2 and Leg 3, the stand-off height data was collected for three packages on one board only. There is a large variation in the stand-off height for each leg, with the range being over 8mils from smallest to largest value for Leg 1 solder joints and about 5 mils for Leg 2 and Leg 3 solder joints. Leg 2 and Leg 3 solder joints have similar stand-off heights since those solder joints have attained full collapse during the reflow soldering process. Leg 1 has significantly taller solder joints (the mean is about 2 mils higher) than the other two legs, reflecting the partial collapse of these solder joints, since the peak reflow temperature during Leg 1 assembly does not get above the SAC405 solder liquidus temperature.

Figure 8b shows the variation of the solder joint stand-off heights across the three cross-sectioned rows, an outer row, an inner row and a die shadow row, indicated on the ball map of the package test vehicle in Figure 5. This plot is for Leg 1 (partial mixing) assemblies only. Each data point in this graph is a mean of the stand-off height for the same ball numbers from six packages across two assemblies. The reason for the wide range in the stand-off heights is apparent from this plot. Due to the dynamic warpage characteristics of the package test vehicle the solder joints on the outer rows are stretched with tall stand-off heights, whereas those in the inner rows, particularly within the center of the package are compressed (squashed) with short stand-off heights.

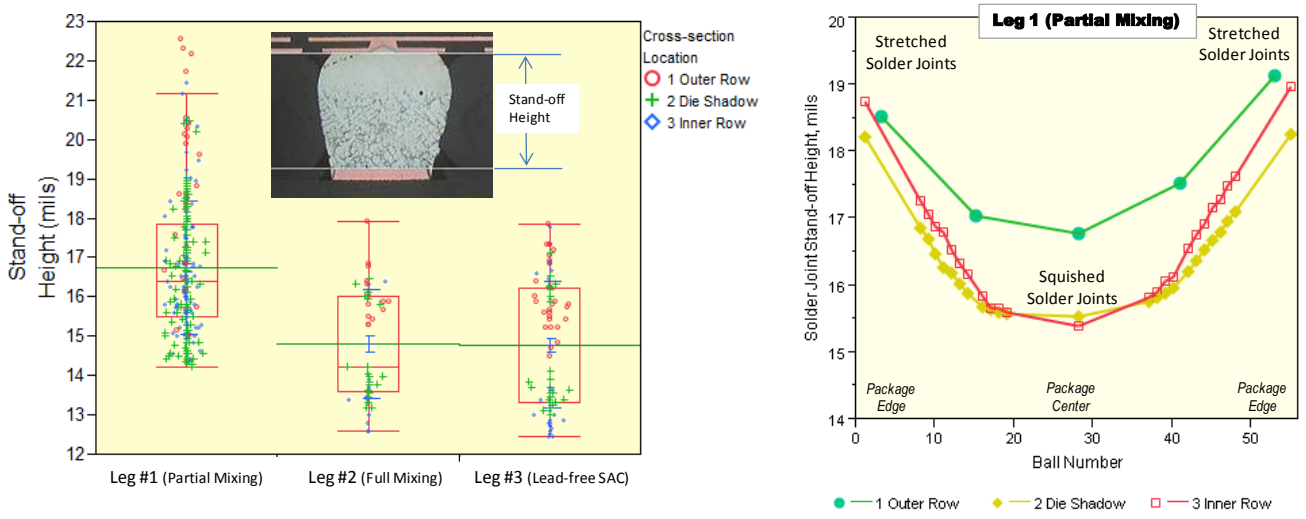

(a) (b)

Figure 8: (a) Stand-off heights of the BGA solder joints for all three Legs of the experiment; the inset micrograph depicts the measurement of the stand-off height. (b) Variation of the stand-off heights of the BGA solder joints for Leg 1 (Partial Pb mixing) assemblies across the outer, die shadow and inner rows.

Figure 9 is a compendium of single solder joint micrographs from each of the three legs, for each of the three cross-section cut locations (outer row, inner row, die shadow row). The variation of the solder joint stand-off heights are apparent with the center solder joints compressed whereas the edge solder joints are stretched, especially in the inner and die shadow rows. The variations in the leg mixing levels are also apparent, with Leg 1 having partial Pb mixing with this level varying from edge to center and from row to row. Leg 2 has full Pb mixing for all solder joint locations on all rows.

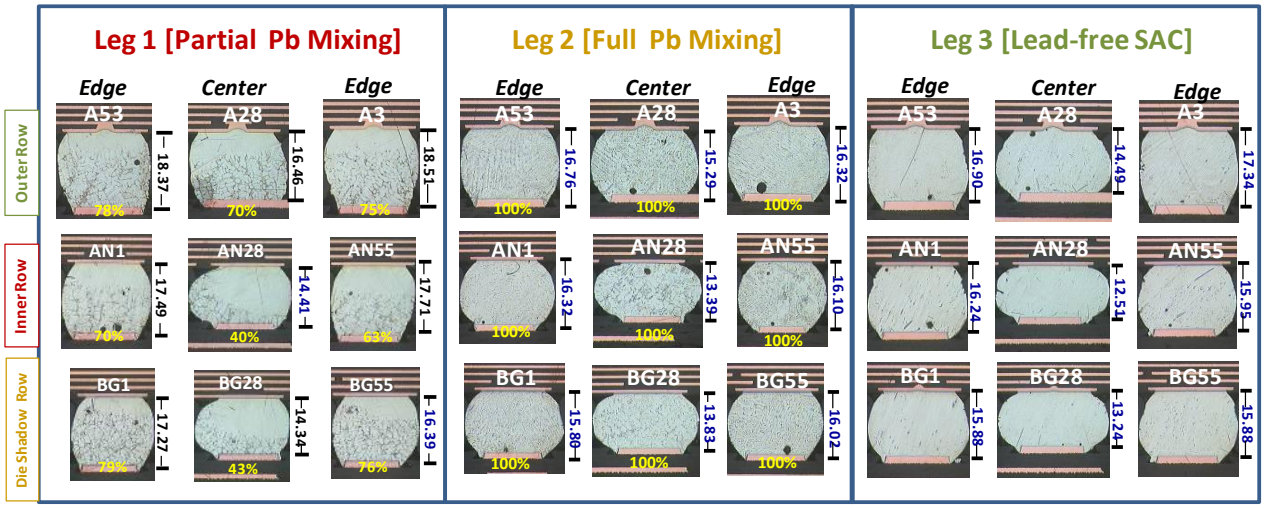

Figure 9: A collection of typical single solder joint micrographs for from each of the three legs, and for each of the three cross-section cut locations. Ball numbers, %Pb mixing levels and stand-off height in mils for each solder joint are also listed.

Detection of Head-on-Pillow (HoP) Defects

As discussed in the Accelerated Thermal Cycling section below, a number of early solder joint failures were recorded at less than 5 cycles into the test. These failures occurred too early to be fatigue failures. A solder joint quality defect was suspected as the root cause of these early failures.

To confirm this, two package locations on a single board that exhibited the early failures were analyzed using 3D Computer Tomography (CT) X-ray technique. This technique enables detection of solder joint quality issues without destructive cross-sectioning of the sample. Figure 10 shows the X-ray images obtained from two assembled packages on a Leg 3 (Lead-Free SAC) board that had early failures. The images in the top two rows are for two different solder joints from the same package location on the board. The bottom row images are from another package location on the same board. In all three cases, the head-on-pillow defect signature is clearly visible. The left images are in 3D view with multiple solder joints visible. The right images are various slices of the single solder joint that had the defect. This analysis confirmed that the HoP defect was the root cause of the early failures during the accelerated thermal cycling tests for these boards.

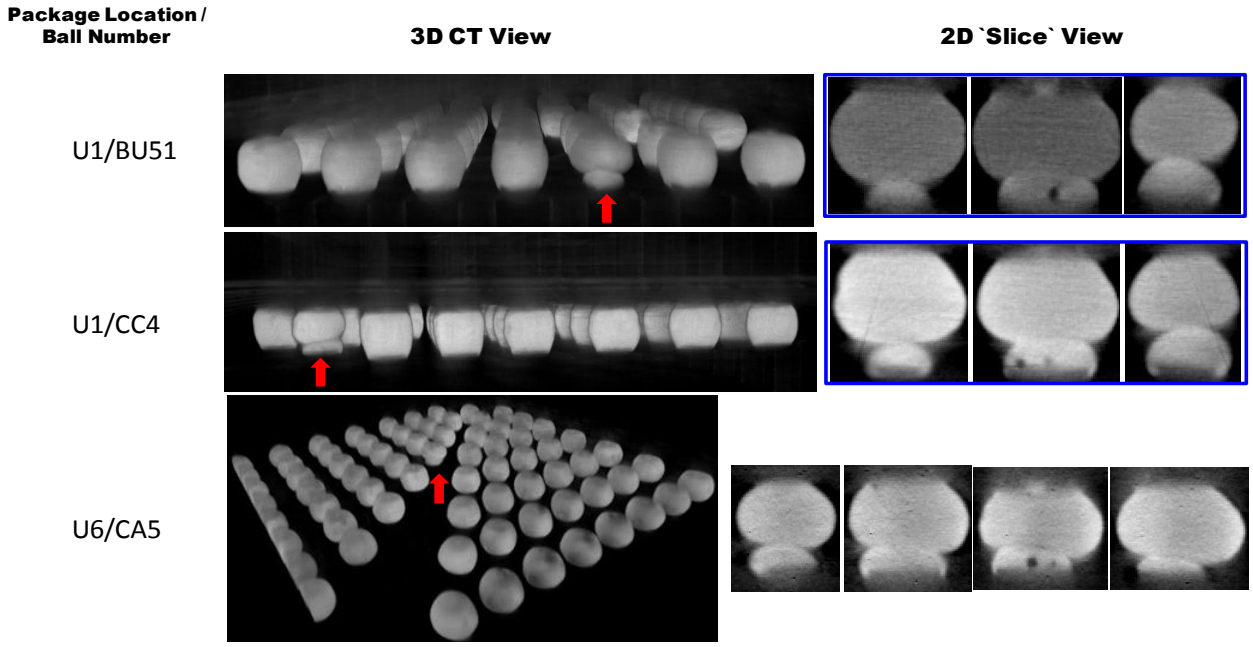

Figure 10: 3D CT and 2D slice X-ray images depicting Head-on-Pillow (HoP)defects at three solder joint locations for one Leg 3 (Lead-free SAC) board.

Accelerated Temperature Cycling (ATC)

The components and the test circuit boards were daisy chained to allow electrical continuity testing after surface mount assembly and in situ, continuous monitoring during thermal cycling. The resistance of each loop was independently monitored during the temperature cycle test. All assembled circuit boards were thermally cycled from 0 °C to 100 °C (10 minute ramp between temperature extremes with a 10 minute dwell time at each temperature extreme) in accordance with the IPC-9701A industry test standard [51]. The solder joints were monitored continuously during thermal cycling with an event detector set at a resistance limit of 1000 ohms. A spike of 1000 ohms for 0.2 microseconds followed by 9 additional events within 10% of the cycles to the initial event is flagged as a failure. The failure data are reported as characteristic life η (number of cycles to 63.2% failure) and slope β from a two-parameter Weibull analysis.

Microstructural Characterization and Failure Analysis

A baseline characterization was performed on representative board level assemblies from each test cell. These baselines were performed to document the microstructures and level of Pb mixing before temperature cycling and to enable comparisons to samples removed from the temperature cycling chambers for failure analysis. Microstructural characterization and failure analysis were done with optical microscopy and scanning electron microscopy (SEM). Backscattered electron imaging (BEI) was the primary technique used to characterize the Pb mixing. Optical metallography (cross-sectional analysis) was used to verify the failure mode. Optical metallography is adequate for most SnPb assessments but the SEM used in the backscattered electron imaging (BEI) mode has proven to be very useful for differentiating Pb-rich phases [3] and intermetallic compounds in the SAC microstructures [45, 49, 50].

RESULTS AND DISCUSSION

Accelerated Temperature Cycling (ATC) – Early Failures

The data for Pb mixing solder standoff, and warpage presented previously in the process characterization section exemplify the assembly challenges inherent to this large BGA package. These assembly challenges are reflected in the thermal cycling results shown in Table 2. A total of 15 early failures were reported and in most cases, the failures occurred within the initial five cycles of the testing. A comparison of censored vs. uncensored sample sizes in Table 2 shows that a number of early failures occurred in each of the three test cells (Legs 1, 2, and 3). The root cause of the early failures was determined through metallographic cross sectional failure analysis. The optical photomicrographs in Figure 11 show the source of the open circuit failure, a head-on-pillow (HoP) defect [52], as well as stretched solder joints resulting from dynamic warpage of the BGA package. These failures are not surprising given the wide range of assembly quality shown in Figures 8-10.

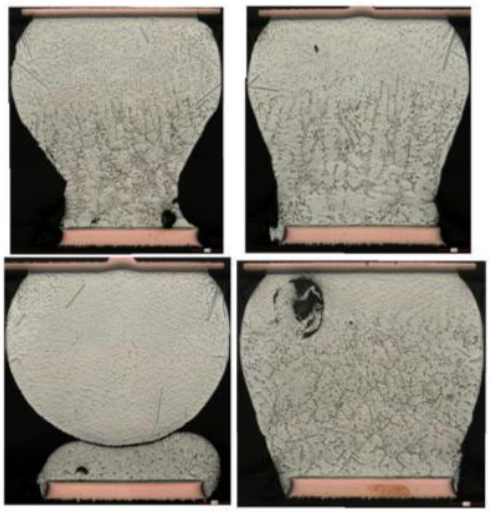

Figure 11: Optical photomicrographs of a temperature cycled Leg 1 BGA test vehicle showing examples of necked-down and stretched solder joints and a head-on-pillow defect that resulted in an early failure condition.

Accelerated Temperature Cycling (ATC) – Thermal Fatigue Failures

The temperature cycling data for the 3162 ball count BGA test cells are summarized in Table 2 and presented in the Weibull plot in Figure 12. The Weibull plot presents only censored data, with the early, non-fatigue failures removed. The parameter used to assess the reliability or thermal fatigue performance is the Weibull characteristic fatigue lifetime (η). For these three test cells, the Leg 1 Partial % Pb Mixing cell has better reliability than either the Leg 2 Full Pb Mixing cell or the completely Pb-free SAC405 cell. Additionally, the full Pb mixed cell (Leg 2) has approximately 10% better reliability than the SAC405 Pb-free cell (Leg 3).

There are two interesting findings that emerge from the characteristic lifetime data. First, these data indicate that introducing a moderate amount of Pb into the solder joints generally does not reduce the thermal fatigue reliability of the SAC405 solder joints. Second, the test cell with partial Pb mixing outperforms both the full Pb mixed cell and the pure (no Pb) SAC405 cell. These findings are interesting considering the results of previous studies that have shown that solder fatigue reliability of partial or fully mixed alloy assemblies is comparable to that of pure SAC assemblies [3, 6, 11, 49]. When differences have been reported, they have been no more than $\pm$ 5-10%, which is regarded to be approaching or within experimental error. In this experiment, a much greater difference is observed with the Leg 1, partial Pb mixed cell outperforming the pure SAC405 cell by approximately 25%. Results from a recent study suggest that the thermal fatigue resistance of mixed alloy (backward compatible) solder joints may be controlled more by the characteristics and properties of the underlying Pb-free (SAC) microstructure than by the Pb content [49]. It is known that differences in SAC microstructure in turn, can result from differences in surface mount assembly parameters such as peak temperature and cooling rate. The following section on **Failure Analysis and Microstructural Evolution** explores the relationship between microstructure and Pb mixing parameters.

Table 2: Weibull statistics summary for thermal cycling 3162 ball count BGA mixed alloy assemblies.

Test Cell	Initial Sample Size	Censored Sample Size*	Characteristic Life η (cycles)	Slope β	Correlation Coefficient r^2
Leg 1 Partial % Pb Mixing	32	26	5795	10.8	0.975
Leg 2 Full Pb Mixing	32	28	4758	14.0	0.965
Leg 3 Pb-free SAC405	32	27	4382	10.2	0.818
*Note: Censoring the early failure data points reduced the effective sample size to less than 32.					

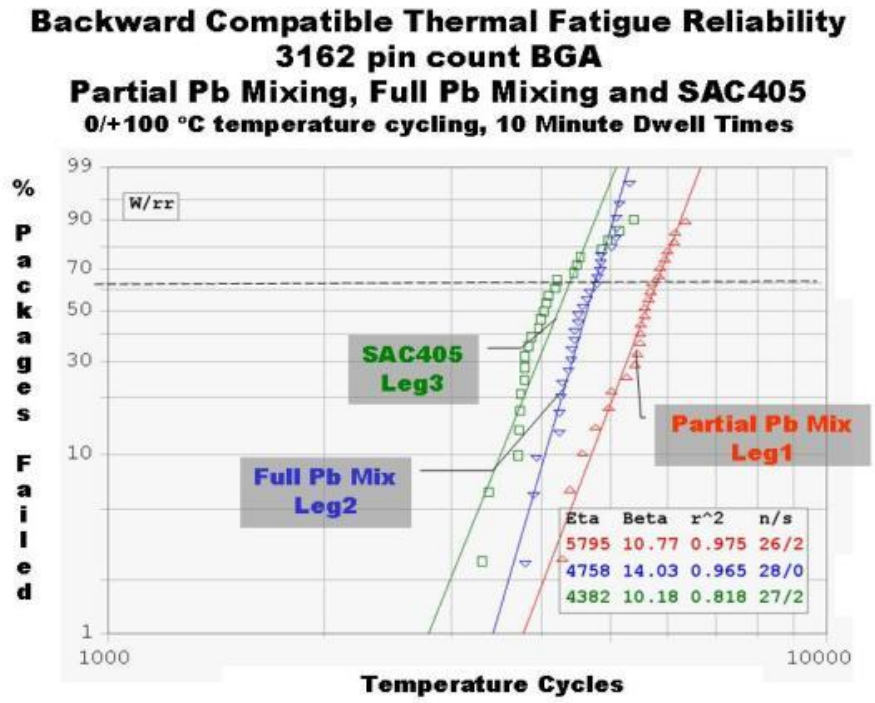

Figure 12: Weibull plot comparing the temperature cycling performance of mixed alloy Leg 1 (partial Pb mixing) and Leg 2 (full Pb mixing) and the Pb-free Leg 3 (SAC405, no Pb mixing).

Microstructural Characterization and Failure Analysis

Baseline Microstructural Characterization

Metallographic analyses were performed to characterize the microstructure of the two backward compatible mixed alloy assemblies (Leg 1 and Leg 2) and the pure SAC405 assembly (Leg 3). The same metallographic techniques subsequently were applied to characterize and analyze the failures from the ATC tests.

Figure 13 shows a number of backscattered electron images (BEI) of the baseline microstructures for typical BGA samples from each of the test cells used in the mixed alloy accelerated temperature cycling study. In the backscattered mode, the dense, Pb-rich phase has a bright white appearance. Figure 13a shows details of the partially mixed microstructure (Leg 1) that results from assembly using a SnPb soldering profile with a short TAL and a peak temperature slightly below the Pb-free solder melting point. The Pb has mixed upward through approximately 25-80% of the height of the solder ball, depending on its location in the package (see details in Figures 7 and 9). In the upper region of the solder ball (package side) where the fatigue cracks tend to propagate, the SAC microstructure (without Pb) is more typical of the microstructure found in an as-received BGA before surface mount assembly. The SAC solder in this region did not melt during the surface mount reflow process. The microstructure consists of small primary Sn cells surrounded by regions where the binary Sn-Ag eutectic decomposition has produced dense networks of very fine Ag_3Sn intermetallic particles.

Figure 13b shows the full Pb mixed microstructure (Leg 2) that results from assembly with a SnPb solder profile using longer TAL and temperature slightly above the Pb-free soldering melting point. The Pb from the solder paste is distributed throughout the SAC solder ball during reflow, extending upwards from the PCB pad to BGA pad side of the solder joint. This is characterized as a fully mixed condition but the Pb-bearing constituents are not distributed homogeneously throughout the solder joint. The SAC microstructure again consists of primary Sn grains with Ag_3Sn intermetallic particles at the cell boundaries. However, in this case the Ag_3Sn intermetallic particles have a lamellar, rather than equiaxed morphology. This intermetallic morphology is also found in the reflowed region of Leg 1 and appears to result from using a SnPb assembly profile.

Figure 13c shows the microstructure of the pure Pb-free SAC405 (Leg 3) test cell created with a Pb-free soldering profile using a peak temperature of approximately 240 °C. The pure Pb-free Leg 3 microstructure qualitatively is similar to the microstructure of Leg 1 shown in Figure 13a with primary Sn cells with Sn-Ag eutectic decomposition at the boundaries. The major microstructural difference is that Leg 3 has a lower the density of Ag_3Sn intermetallic particles and the intermetallic particle size is larger.

In these samples, unlike some of the non-optimum solder joints cited in Figure 9-11, the extent of solder melting and mixing has resulted in reasonable solder joint quality. The mixed alloy solder ball collapse is comparable to the pure Pb-free collapse, the solder joints are well-formed, and there is no excessive segregation of Pb in the mixed regions.

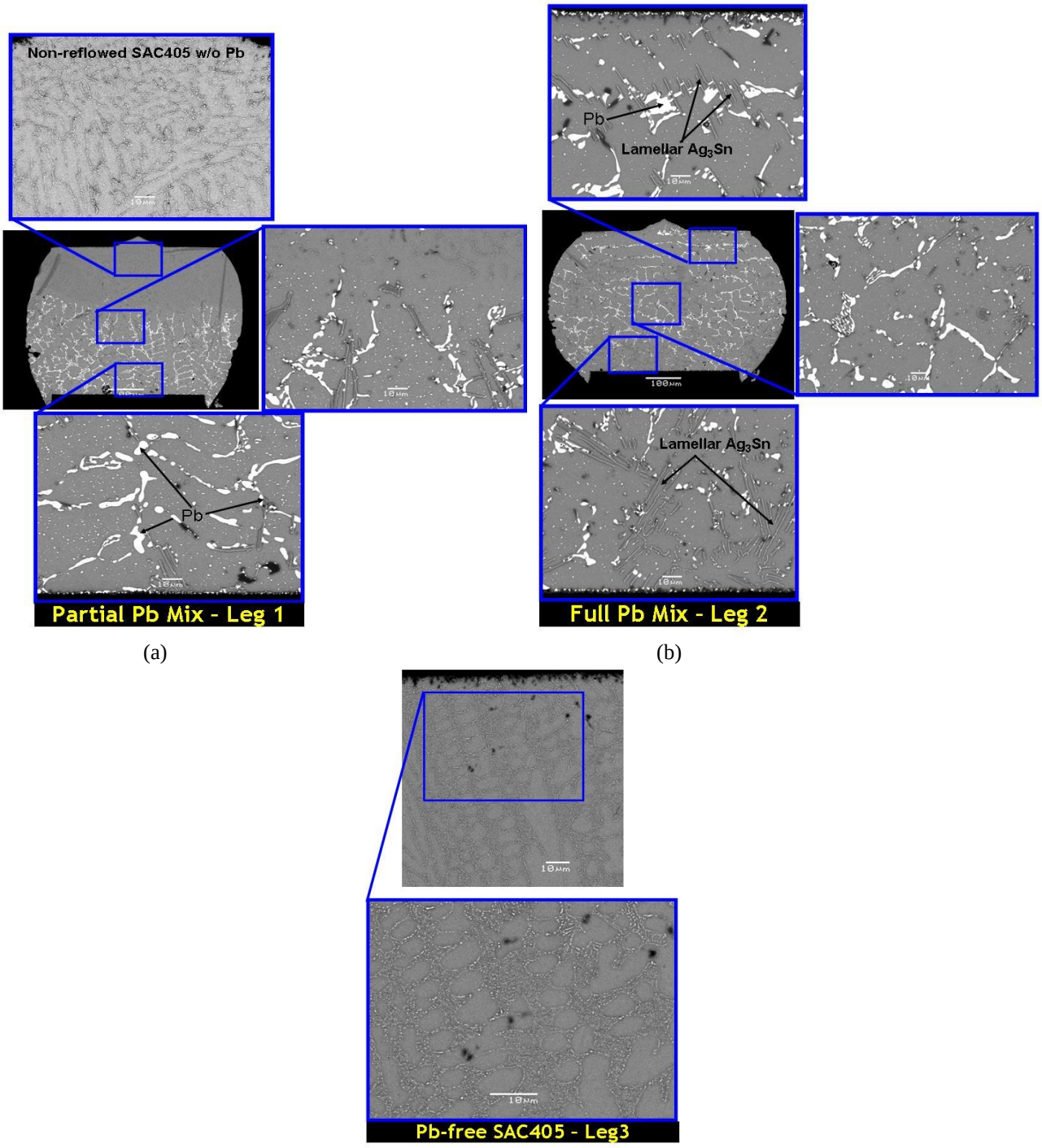

Figure 13: Backscattered electron (BEI) images of the baseline microstructures for typical BGA samples from each of the test cells used in the mixed alloy accelerated temperature cycling study.

Failure Analysis and Microstructural Evolution

Figure 14 shows optical photomicrographs of failed solder joints from the ATC testing. All failures have the characteristic intergranular fracture along Sn boundaries that is seen routinely in SAC fatigue failures and is consistent with those reported much earlier by workers such as Dunford [53]. The fractures in both the partially mixed (Leg 1) and full mixed (Leg 2) samples also resemble SAC fractures because the cracks propagate along Sn boundaries, regardless of the presence of Pb, in the same manner as in the Pb-free sample (Leg 3) [49].

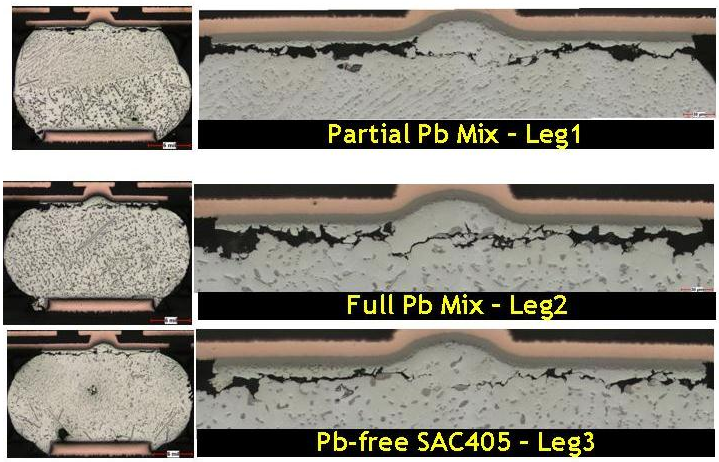

Figure 14: Optical photomicrographs of BGA solder joints from Legs 1, 2, and 3 that have failed by thermal fatigue during accelerated temperature cycling.

Figure 15 shows backscattered electron images of a Leg 1 sample that failed in thermal cycling. Although the initial microstructure had approximately 50% Pb mixing, Pb did not influence the failure because cracking occurred in the upper, Pb-free region (see baseline microstructure in Figure 13a). The higher magnification images show accelerated coarsening of the Ag_3Sn intermetallic particles in the strain-localized region of the solder joint where crack propagation occurs. This pattern of microstructural evolution is characteristic of the thermal fatigue failure process in these Pb-free alloys [54] and was first reported by Dunford in 2004 [53]. The coarsening process is slower in the region below the fatigue crack because it is only driven thermally with a minimal contribution due to strain.

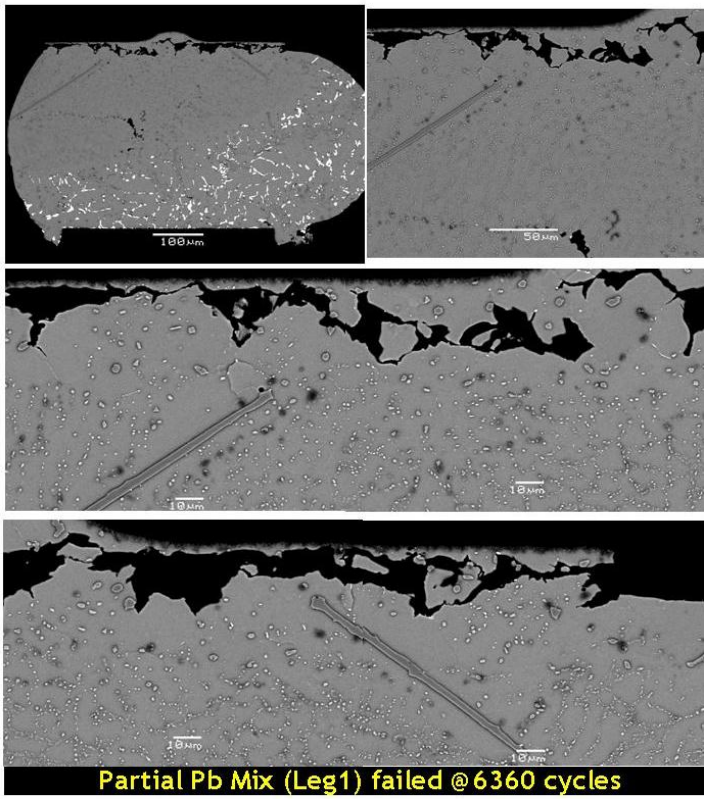

Figure 15: Backscattered electron (BEI) images of a Partial Pb Mix, Leg 1 sample that failed in ATC at 6360 cycles. The fatigue failure occurred at the package side of the solder joint at a significant distance from the region of Pb mixing.

Figure 16 shows backscattered electron images of a Leg 2 sample that failed in thermal cycling. The higher magnification images show coarsening of the lamellar Ag_3Sn intermetallic particles in the strain-localized region of the solder joint where crack propagation occurs. The lamellar morphology remains intact outside the strain-localized region. The crack propagation

path is intergranular along Sn boundaries, as seen routinely in SAC fatigue failures. There are some Pb particles along the crack path but it is difficult to ascribe a negative affect to the presence of Pb since Leg 2 outperformed the Leg 3, Pb-free SAC405 test cell (Figure 12).

Figure 17 shows backscattered electron images of a Leg 3 sample that failed in thermal cycling. As expected, the higher magnification images show Ag_3Sn intermetallic particle coarsening in the strain-localized region of the solder joint and intergranular crack propagation along Sn boundaries.

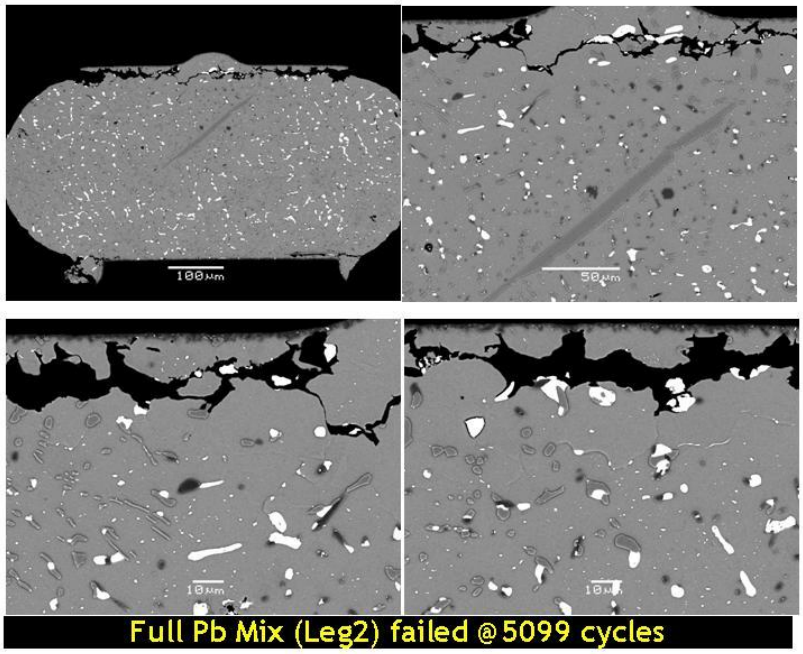

Figure 16: Backscattered electron (BEI) images of a Full Pb Mix, Leg 2 sample that failed in ATC at 5099 cycles.

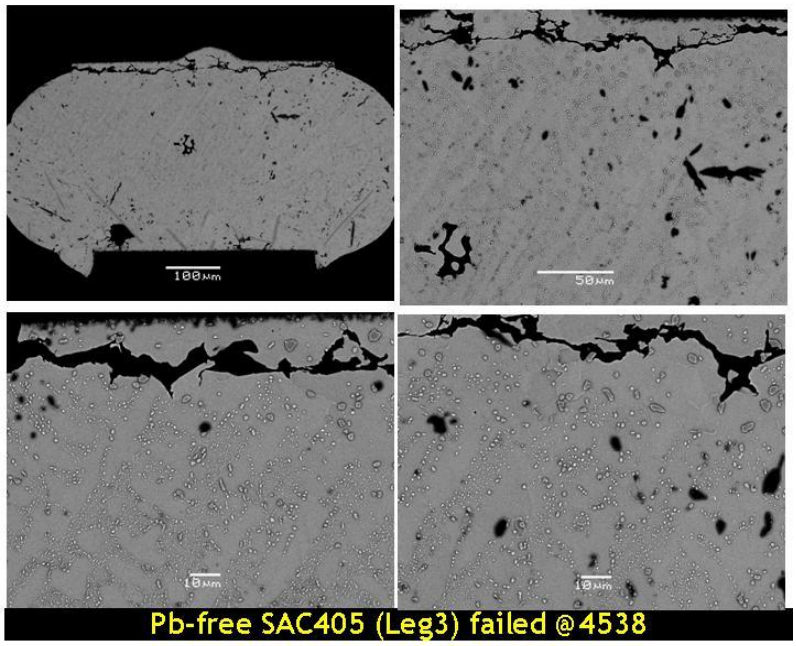

Figure 17: Backscattered electron (BEI) images of a Pb-free SAC405, Leg 3 sample that failed in ATC at 4538 cycles.

The better fatigue resistance of the two mixed alloy test cells was not expected, although a similar result was reported in an earlier study by some of the current authors [50]. This was true particularly in the case of the superior performance of the Partial Pb Mixed Leg 1. Previously it was mentioned that the thermal fatigue resistance of mixed alloy solder joints may be

controlled more by the characteristics and properties of the underlying Pb-free (SAC) microstructure than by the Pb content added during assembly [49]. Figure 18 shows the underlying baseline SAC microstructures and the microstructures after thermal cycling the for the three test cells. Since Legs 1 and 3 both failed in a Pb-free region of their solder joints, a comparison of these two samples is of high interest.

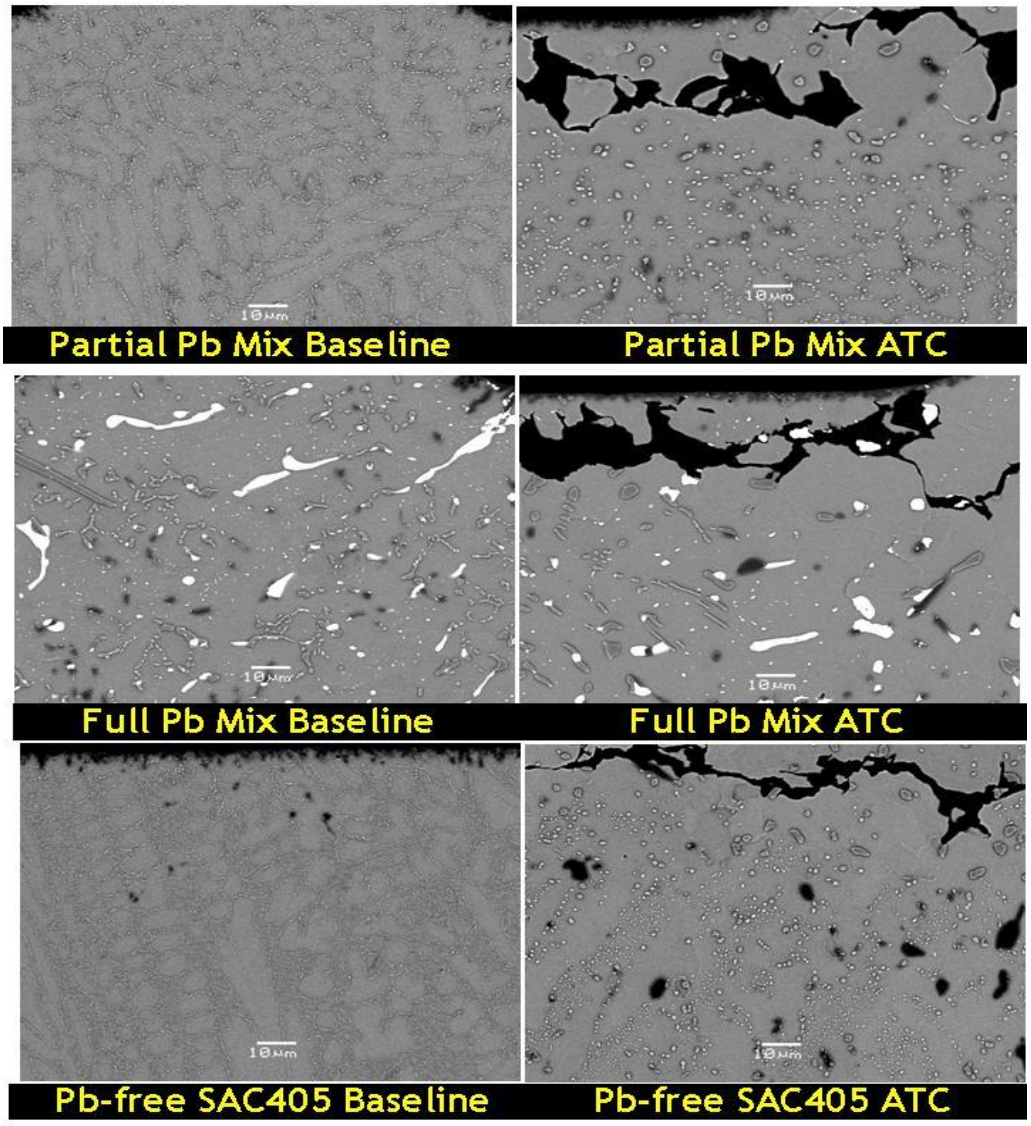

Figure 18: Backscattered electron (BEI) images comparing the baseline SAC microstructures and the microstructures after thermal cycling (ATC) for each of the three test cells.

The higher magnification images in Figure 19 reveal no startling baseline microstructural differences between Leg 1 and Leg 3. The microstructures of both test cells have a high density of the Ag_3Sn intermetallic particles, which is a characteristic of the SAC405 alloy. The quantity and size of the Ag_3Sn intermetallic particles is similar in both samples, although the Leg 1 sample may contain a slightly higher volume fraction of Ag_3Sn particles. A higher volume fraction of Ag_3Sn particles could account for the better fatigue resistance in Leg 1 [55, 56, 57]. The Leg 3 sample appears to contain larger primary Sn dendrites, and there is one paper that suggests fatigue resistance increases with increasing Sn dendrite size [58]. The Sn dendrite effect however, remains only a hypothesis and has not been supported by other research. A definitive determination of Sn dendrite and intermetallic particle size and distribution would require extensive quantitative metallography, which is beyond the scope of this study.

There is one study in the literature that suggests that the lamellar Ag_3Sn intermetallic morphology present in Leg 2 resists particle coarsening and provides a moderate increase in fatigue resistance [45]. In the current work however, there does not appear to be a correlation between the lamellar microstructure and fatigue life because Leg 2 outperforms Leg 3 but does not

outperform Leg 1. In summary, the findings in the current metallographic and microstructural analysis are not alone sufficient to explain the better fatigue resistance of the two mixed alloy test cells.

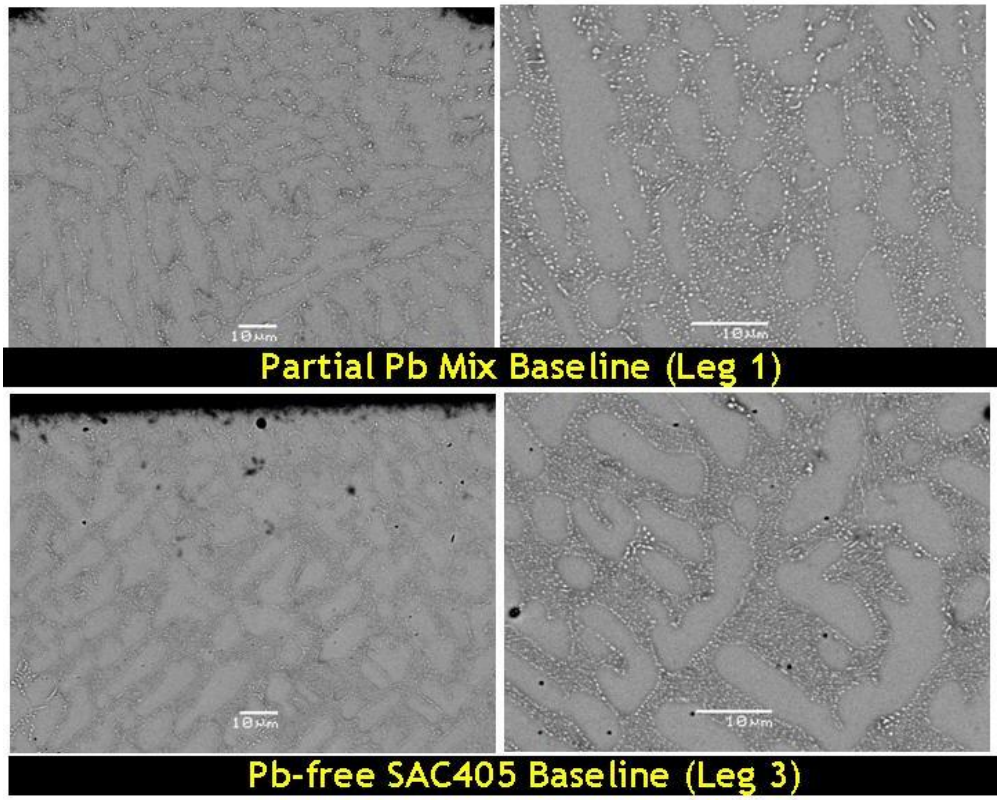

Figure 19: Higher magnification backscattered electron (BEI) images comparing the baseline SAC microstructures of the Leg 1 partial %Pb Mix Leg 3 Pb-free test cells.

Discussion of ATC Results

Although the mixed alloy thermal *fatigue results* for Legs 1 and 2 certainly are better than expected, they do not constitute an endorsement of mixed alloy, backward compatible assembly for this large body, high pin count BGA. The censored data in Table 2 and the early failure mode shown in Figure 11 emphasize the primary finding of this study: 15% of the samples submitted for thermal cycling failed almost immediately in testing. It is true that early failures also plagued the Pb-free samples (no Pb mixing) but that is a clear indication of the impact of the inherent package warpage on assembly quality. It should seem obvious that adding Pb mixing to an already risky assembly process would only further increases the risk. This conclusion is validated by the substantial variation in %Pb mixing and overall quality in the Leg 1 samples driven by dynamic package warpage, large thermal mass, and the unusually large physical dimensions and high pin count of the package.

The better thermal fatigue performance of the Pb mixed alloy test cells could be due to a combination of factors. The results of the microstructural analysis hinted that the Ag_3Sn intermetallic particle density might be greater in Leg 1, but this is a tentative observation, not a strong correlation. It should also be noted that due to the *de facto* industry standardization of SAC305, very few of the recent mixed alloy experiments have studied detailed microstructural effects in higher Ag content alloys such as SAC405. Therefore previous results on SAC305 may not be directly applicable to SAC405. The dynamic warpage of the package in Leg 1 may also lead to a larger average solder joint standoff heights (Figures 9 and 11) thereby increasing fatigue life moderately.

It also is worth mentioning that the testing parameters could influence the test results. Microstructure related differences in fatigue performance tend to be manifested more in thermal cycling tests run with shorter dwell times such as the 10 minute dwell used in the current study [50]. Conversely, longer dwell times have been shown to minimize or eliminate effects related to the initial microstructure [45, 49]. The apparent differences in fatigue life between the SAC405 and the mixed cells could diminish if a longer test dwell time was applied. This has practical implications because longer dwells are more characteristic of actual service conditions.

Factors Affecting Solder Joint Quality

There are many design and surface mount assembly parameters that can modulate the solder joint quality and solder joint defect types. These factors include package substrate and printed circuit board thicknesses, form factor, material properties of the component, PCB, solder alloy, and SMT process parameters such as reflow profile, stencil aperture size and thickness, printed solder paste volume on the PCB lands, and fixturing. Typical solder joint defects include solder bridging, Head on Pillow (HoP), Non Wet Opens (NWO), solder dewetting, and excessive solder voids. In this study, HoP and elongated solder joints were observed often as shown in Figures 10 and 11. The HoP defect typically forms when there is poor contact between the solder ball at the component side and solder paste at the board side during melting and solidification through the reflow profile. Any ball that solidifies quickly with less time to wet the paste or contact molten solder at the PCB side during cooling is likely to form a HoP defect. Local board warpage and variations in paste volume and paste activity can modulate the defect levels. The magnitude of the component warpage is a function of package size [59, 60] and certain SMT factors (increasing the paste volume for the affected PCB pads and use of higher activity paste) were able to reduce or eliminate HoP defects in this study.

Conclusions

The fundamental conclusion of this study is that solder joint quality issues need to be first addressed and resolved before attempting mixed alloy assembly on thermally massive BGA packages or packages. The following detailed conclusions can be drawn from the results of the mixed alloy assembly and thermal cycling study:

- The thermal cycling data indicates that introducing a moderate amount of Pb into the solder joints does not reduce the thermal fatigue reliability of the SAC405 solder joints. The thermal fatigue crack path in the Pb mixed joints is intergranular along Sn boundaries and has a similar appearance to the cracking in the pure Pb-free SAC405 solder joints. The failure mode and cracking mechanism are consistent with results reported in previous studies.
- The thermal cycling data show that the test cell with partial Pb mixing outperforms both the full Pb mixed cell and the pure (no Pb) SAC405 cell. These findings appear to contradict the results from previous studies that show that solder fatigue reliability of partial or fully mixed alloy assemblies is comparable to that of pure SAC assemblies. The better performance of the Pb mixed test cells could be attributed to differences in surface mount profile, particularly differences in peak temperature and TAL. Different soldering profiles can produce different solidification conditions that in turn, result in different basic SAC microstructures, different warpage profiles, and different solder standoff heights.
- The high thermal mass and large physical dimensions of some BGA packages may limit the ability to create fully Pb mixed solder joints with a nominal SnPb reflow assembly profile. When a typical SnPb peak temperature and time above liquidus (TAL) is employed, it is difficult to achieve full Pb mixing at any package location and the partial %Pb mixing varies by as much as a factor of 2 across the BGA package. It must be noted that in practice, operating at temperatures above the nominal SnPb processing window can damage other components on the printed circuit board assembly and can diminish the effectiveness of the flux in the solder paste.

Acknowledgments

The authors want to acknowledge the following people for their valuable contributions and comments: the management support of Marc Benowitz and Sherwin Kahn from Alcatel-Lucent Bell Labs Reliability; the management support of Tom Clawson and Mulugeta Abtew of Sanmina-SCI and the PCB assembly support provided by the Sanmina-SCI(Guadalajara, MX) NPI team; the management support of Michael Stark of Intel's Customer Platform Technology Development Team.

References

[1] "Annex to Directive 2002/95/EC, Restriction on the use of hazardous substances (RoHS) in electrical and electronic equipment," *Official Journal of the European Union*, 14.10.2006, L283/48-49, October 12, 2006.

[2] *iNEMI Availability of SnPb-Compatible BGAs Workshop*, Cupertino, CA, March 1, 2007. http://www.inemi.org/cms/projects/ese/SnPb_BGAs.html

[3] Richard Coyle, Peter Read, Steven Kummerl, Debra Fleming, Richard Popowich, and Indraneel Chatterji, "A Comprehensive Analysis of the Thermal Fatigue Reliability of SnPb and Pb Free Plastic Ball Grid Arrays (PBGA) Using Backward and Forward Compatible Assembly Processes," *SMT Journal*, Volume 21, Issue 4, 33-47, October-December, 2008.

[4] B. Smith, P. Snugovsky, M. Brioux, and A. Grivon, "Industrial Backward Solution for Lead Free Exempted AHP Electronic Products, Part 2: Process Technology Fundamentals ands Failure Analysis," *Proceedings of APEX 2008*, S15-01, Las Vegas, NV, 2008.

[5] P. Snugovsky, H. McCormick, S. Bagheri, Z. Bagheri, C. Hamilton, and M. Romansky, "Microstructure, Defects, and Reliability of Mixed Pb free/SnPb Assemblies," *Supplemental Proceedings: Volume I: Materials Processing and Properties TMS (The Minerals, Metals, and Materials Society*, 631-642, New Orleans, LA, 2008.

[6] Robert Kinyanjui, Quyen Chu, Polina Snugovsky, Richard Coyle, "Solder Joint Reliability of Pb-free SnAgCu Ball Grid Array (BGA) Components in SnPb Assembly Process," *Proceedings of APEX 2008*, S15-02, Las Vegas, NV, 2008.
[7] Robert Kinyanjui and Quyen Chu, "The Pb-free SnAgCu Ball Grid Array (BGA) Components in SnPb Assembly Process: Process Characterization and Solder Joint Reliability," *Proceedings of SMTAI*, 760-769, Orlando, FL, 2007.
[8] H. McCormick, P. Snugovsky, C. Hamilton, Z. Bagheri, and S. Bagheri, "The Great SAC Debate: The Reliability of SAC305 and SAC405 Solders in a Variety of Applications," *Proceedings of PanPac Symposium*, 333-341, January 31, 2007.
[9] J. Nguyen, D. Geiger, D, Rooney, and D. Shangguan, "Backward Compatibility Study of Lead-Free Area Array packages with Tin-Lead Soldering Processes," *Proceedings of APEX*, S09-03, Anaheim, CA, 2006.
[10] J. Nguyen, D. Geiger, D, Rooney, and D. Shangguan, "Reliability Study of Lead-Free Area Array Packages with Tin-Lead Soldering Processes," *Proceedings of SMTAI*, 433-438, Chicago, IL, 2006.
[11] H. McCormick, P. Snugovsky, Z. Bagheri, S. Bagheri, C. Hamilton, G. Riccitelli, and R. Mohabir, "Mixing Metallurgy: Reliability of SAC Balled Area Array Packages Assembled Using SnPb Solder," *Proceedings of SMTAI*, 425-432, Chicago, IL, 2006.
[12] A. Zbrzezny, P. Snugovsky, T. Lindsay, R. Lau, "Reliability Investigation of Mixed BGA Assemblies"; *IEEE Transactions on Electronic Package Manufacturing*, vol. 29, no.3, 211-216, July, 2006.
[13] O. Maire, C. Munier, S. Bousquet, C. Chastenet, and M. Jeremias, "Backward Compatibility of Lead-Free BGA: Microstructural Characterization and Reliability," *Proceedings IPC Soldertec*, Malmo, Sweden 2006.
[14] C. Hunt and M. Wickham, "Impact of Lead Contamination on Reliability of Lead Free Alloys," *Proceedings IPC Printed Circuits Expo 2006*, S39-01, 2006.
[15] I. Chatterji, "Backward Compatibility, Are We Ready- A Case Study"; *Proceedings of SMTAI*, 416-424, Chicago, IL, 2006.
[16] M. Abtew, R. Kinyanjui, N. Nuchsupap, T. Chavasiri, N. Yingyod, P. Saetang, J. Krapun, and K. Jikratoke, "Effect of Inert Atmosphere Reflow and Solder Paste Volume on the Microstructure and Mechanical Strength of Mixed Sn-Ag-Cu and Sn-Pb Solder Joints," *Proceedings of SMTAI*, 74-78, Chicago, IL, 2006.
[17] H. McCormick, P. Snugovsky, Z. Bagheri, and S. Bagheri, "Pb-free Test Vehicle, Microstructure and ATC Behavior of SAC305 and SAC405 BGAs Assembled with SnPb Solder," *Proceedings of International Conference on Lead-free Soldering*, Toronto, ON, Canada, no. 11, 1-9, May 16-18, 2006.
[18] A. Giamis, G. Wenger, and P. Solan, "Mixed Alloy Solder Joint Reliability Sanity Check," *Proceedings of International Conference on Lead-free Soldering*, Toronto, ON, Canada, no. 12, 1-5, May 16-18, 2006.
[19] Woodrow, T.A., "JCAA/JG-PP Lead-Free Solder Project: -20 to +80 °C Thermal Cycling Test", *Proceedings SMTA International*, 825-835, Rosemont, IL, September 24-28, 2006.
[20] A. Zbrzezny, P. Snugovsky, T. Lindsay, R. Lau, "Reliability Investigation of Mixed Solder Interconnects – Case Studies," *Proceedings of SMTAI*, 397-402, Chicago, IL, 2005.
[21] H. McCormick, P. Snugovsky, Z. Bagheri, S. Bagheri, C. Hamilton, G. Riccitelli, and R. Mohabir, "Mixing Metallurgy: Reliability of SAC Balled Area Array Packages Assembled Using SnPb Solder," *SMTA Journal*, Vol. 20, no. 2, 11-18, 2007.
[22] P. Snugovsky, A. R. Zbrzezny, M. Kelly, M. Romansky, "Theory and Practice of Lead-Free BGA Assembly Using Sn-Pb Solder," *Proceedings CMAP (Centre for Microelectronics Assembly and Packaging in Canada) International Conference on Lead-free Soldering*, University of Toronto, Toronto, ON Canada, May 2005.
[23] J. Bath, S. Sethuraman, X. Zhou, D. Willie, K. Hyland, K. Newman, L. Hu, D. Love, H. Reynolds, K. Kochi, D. Chiang, V. Chin, S. Teng, M. Ahmed, G. Henshall, V. Schroeder, Q. Nguyen, A. Maheswari, M. Lee, J-P Clech, J. Cannis, J. Lau, C. Gibson, "Reliability Evaluations of Lead-Free SnAgCu PBGA676 Components Using Tin-Lead and Lead-Free SnAgCu Solder Paste," *Proceedings of SMTAI*, 891-901, Chicago, IL, September 25-29, 2005.
[24] D. Hillman, M. Wells, and K. Cho, "The Impact of Reflowing a Pb-free Solder Alloy using a Tin/Lead Solder Alloy Reflow Profile on Solder joint Integrity," *Proceedings CMAP (Centre for Microelectronics Assembly and Packaging in Canada) International Conference on Lead-free Soldering*, University of Toronto, Toronto, ON Canada, May 2005.
[25] J. L. Evans, C. Mitchell, M. Bozak, L. N. Payton, M. R. McQuenney, and J. R. Thompson, "Reliability of SAC BGA Using SnPb Paste for Harsh Environment Electronics," *Proceedings of SMTAI*, 365-370, Chicago, IL, September 25-29, 2005.
[26] B. Nandagopal, Z. Mei, and S. Teng, "Microstructure and Thermal fatigue Life of BGAs with Eutectic Sn-Ag-Cu Balls Assembled at 210 °C with Eutectic Sn-Pb Paste," *Proceedings of Electronic Component and Technology Conference*, 875-883, San Diego, CA, 2006.
[27] B. Nandagopal, D. Chiang, S. Teng, P. Thune, L. Anderson, R. Jay, and J. Bath, "Study on Assembly, Rework Process, Microstructures and Mechanical Strength of Backward Compatible Assembly," *Proceedings of SMTAI*, 861-870, Chicago, IL, September 25-29, 2005.
[28] Gunter Grossmann, Joy Tharian, Pascal Jud, and Urs Sennhauser, "Microstructural investigation of lead-free BGAs soldered with tin-lead solder," *Soldering & Surface Mount Technology*, vol. 17 no. 2, pp. 10-21, 2005.

[29] C. Handwerker, "Transitioning to Pb-free Assemblies," Circuits Assembly; March, 2005.
[30] M. Wickham, L. Zou, M. Dusek, C. Hunt, "Measuring the Reliability of Electronics Assemblies During the Transition Period to Lead-Free Soldering", NPL Report DEPC MPR 030, National Physical Laboratory, UK August 2005.
[31] Peter Borgesen, 2005 Year End Report Unovis Area Array Consortium (formerly Universal Instruments Consortium).
[32] Jean-Paul Clech, Lead-Free and Mixed Assembly Solder Joint Reliability Trends, *Proceedings of APEX 2004*, S28-3, Anaheim, CA, February 24-26, 2004.
[33] C. Handwerker and J. Bath, et al.; "NEMI Lead-Free Assembly Project: Comparison between PbSn and SnAgCu Reliability and Microstructures," *Proceedings of SMTA International*, 2003.
[34] P. Snugovsky, M. Kelly, Z. Bagheri, and M. Romansky, "Lead Free and Lead Bearing Solder Intermetallic Formation on Electroless Ni/Immersion Au Interconnects Affected by Black Pad," *Proceedings of APEX*, S02-1, January 20-24, 2002.
[35] F. Hua, R. Aspandiar, T. Rothman, C. Anderson, G. Clemons, and M. Klier, "Solder Joint Reliability of Sn-Ag-Cu BGA Components attached with Eutectic Pb-Sn Solder Paste" *Journal of Surface Mount Technology*, Volume 16, Issue 1, 34-42, 2003.
[36] F. Hua, R. Aspandiar, T. Rothman, C. Anderson, G. Clemons, C-K. Chung, M. Faizul, "Solder Joint Reliability Assessment of Sn-Ag-Cu BGA Components Attached with Eutectic Pb-Sn Solder," *Proceedings of SMTA International Conference*, 246-252, Chicago, IL, 2003.
[37] C. K. Chung, R. Aspandiar, K. F. Leong, C.S. Tay, "The Interactions of Lead (Pb) in Lead-Free Solder (Sn/Ag/Cu) System," *Proceedings of Electronic Components and Technology Conference*, 166-173, San Diego, CA, May 28-31, 2002.
[38] P. Snugovsky, Z. Baghjeri, M. Kelly, M. Romansky, "Solder Joint Formation with Sn-Ag-Cu and Sn-Pb Solder balls and Pastes," *Proceedings of SMTA International Conference*, SOL3-1, Chicago, IL, Sep 22-26, 2002.
[39] J. Oliver, O. Rod, M. Nylén, C. Markou, "Fatigue Properties of Sn/3.5ag/0.7cu Solder Joints and Effects of Pb-Contamination," *Journal of SMT*, Volume 15, Issue 4, 23-28, 2002.
[40] Karl Seelig and David Suraski, "A Study of Lead-Contamination in Lead-free Electronics Assembly and its Impact on Reliability," *Proceedings of SMTA*, SOL4-3, Chicago, IL, 2002.
[41] J. Bartelo, S. Cain, D. Caletka, K. Darbha, T. Gosselin, D. Henderson, D. King, K. Knadle, A. Sarkhel, G. Thiel, C. Woychik, D. Shih, S. Kang, K. Puttlitz and J. Woods, "Thermomechanical Fatigue Behavior of Selected Pb-Free Solders, IPC *APEX 2001*, LF2-2, January 14-18, 2001.
[42] S. Choi, T. R. Bieler, K. N. Subramanian, J. P. Lucas, "Effects of Pb contamination on the eutectic Sn-Ag solder joint"; *Soldering & Surface Mount Technology*, 13/2, 26-29, 2001.
[43] Q. Zhu, M. Sheng, and L. Luo, "The effect of Pb contamination on the microstructure and mechanical properties of SnAg/Cu and SnSb/ Cu solder joints in SMT," *Soldering & Surface Mount Technology*, 12/3,19-23, 2000.
[44] Paul Vianco, Jerry Rejent, Iris Artaki, Urmi Ray, Donald Finley, and Anna Jackson, "Compatibility of Lead-Free Solders with Lead Containing Surface Finishes as a Reliability Issue in Electronic Assemblies," *Proceedings of Electronic Component and Technology Conference*, 1172-1183, Orlando, FL, May 28-31, 1996.
[45] R. Coyle, M. Reid, C. Ryan, R. Popowich, P. Read, D. Fleming, M. Collins, J. Punch, I. Chatterji, "The Influence of the Pb free Solder Alloy Composition and Processing Parameters on Thermal Fatigue Performance of a Ceramic Chip Resistor," *Proceedings of Electronic Components Technology Conference*, 423-430, San Diego, CA, May 26-29, 2009.
[46] Mark Logterman and Lavanya Gopalakrishnan, "A Product Feasibility Study of Assembling Pb-free BGAs in a Eutectic Sn/Pb Process, *Proceedings of 59th Electronic Component and Technology Conference*, 742-751, San Diego, CA, May 26-29, 2009.
[47] Quyen Chu, Girish Wable, Anthony Babasa, Evan Doxtad, Michael Lapitan, Michael Santos, Josh Solon, Ken Hubbard, Gnyaneshwar Ramakrishna, Greg Henshall, Ahmer Syed, Ranjit Pandher, Chrys Shea, "Low-Silver BGA Assembly Phase I – Reflow Considerations and Joint Homogeneity Third Report: Comparison of Four Low-Silver Sphere Alloys and Assembly Process Sensitivities*," Proceedings IPC APEX 2009*, S05-03, Las Vegas, NV, April 2009.
[48] Robert Kinyanjui, Raiyo Aspandiar, Richard Coyle, Vasu Vasudevan Stephen Tisdale, Jorge Arellano, and Satish Parupalli, "Challenges in Reflow Profiling Large and High Density Ball Grid Array (BGA) Packages Using Backward Compatible Assembly Processes," *Proceedings of IPC APEX 2010*, Las Vegas, NV, xxx, April , 2010.
[49] Richard Coyle, Heather McCormick, Peter Read, Richard Popowich, Debra Fleming, and John Osenbach, "A Reliability Comparison of SAC305 AND SAC105 Plastic Ball Grid Arrays Assembled with Backward Compatible Soldering Processes," *Proceedings of SMTAI 2010*, 68-75, Orlando, FL, October 2010.
[50] Vasu Vasudevan, Richard Coyle, Raiyo Aspandiar, Steve Tisdale, Robert Kinyanjui and Gary Long, "Thermal Cycling Reliability, Microstructural Characterization, and Assembly Challenges Encountered with Backward Compatible Soldering of a Large, High Density Ball Grid Array," *Proceedings of Electronic Components Technology Conference*, IEEE, Piscataway, NJ 2011.
[51] M. Meilunas and P. Borgeson, "Effects of Cycling Parameters on the Thermal Fatigue Life of Mixed SnAgCu/SnPb Solder Joints," *Journal of Electronic Packaging*, ASME, Vol. 133, Issue 2, 2011.

[52] Dudi Amir, Raiyo Aspandiar, Scott Buttars, Wei Wei Chin, Paramjeet Gill, and Kedah Kulim, Kedah, "Head –and – Pillow SMT Failure Modes," *Proceedings of SMTAI 2009*, 409-421, San Diego, CA, October 4-8 2009.
[53] Steve Dunford, Sridhar Canumalla, Puligandla Viswanadham, "Intermetallic Morphology and Damage Evolution under Thermomechanical Fatigue of Lead (Pb)-Free Solder Interconnections," *Proceedings of Electronic Components Technology Conference 2004*, 726-736, June 2004.
[54] J. Manock, R. Coyle, B. Vaccaro, H. McCormick, R. Popowich, D., P. Read., J. Osenbach, and D. Gerlach, "Effect of Temperature Cycling Parameters on the Solder Joint Reliability of a Pb-free PBGA Package," *SMT J.*, vol. 21, no.3, 36, (2008).
[55] S. Terashima, Y. Kariya, T. Hosoi, and M. Tanaka, "Effect of Silver Content on Thermal Fatigue Life of Sn-xAg-0.5Cu Flip-Chip Interconnects," *J. Electron. Mater.* vol. 32, no. 12, 2003.
[56] Gregory Henshall, Jasbir Bath, Sundar Sethuraman, David Geiger, Ahmer Syed, M.J. Lee, Keith Newman, Livia Hu, Dong Hyun Kim, Weidong Xie, Wade Eagar, and Jack Waldvogel, "Comparison of Thermal Fatigue Performance of SAC105 (Sn-1.0Ag-0.5Cu), Sn-3.5Ag, and SAC305 (Sn-3.0Ag-0.5Cu) BGA Components with SAC305 Solder Paste," Proceedings APEX, S05-03, 2009.
[57] Richard Coyle, John Osenbach, Peter Read, Heather McCormick, Debra Fleming, Richard Popowich, Michael Reid, Jeff Punch, Maurice Collins, Robert Kinyanjui, and Steven Kummerl, "Dwell Time, Microstructural Dependencies, and the Interpretation of Thermal Fatigue Test Data of SnPb and Pb-free Solders," *Proceedings of SMTAI 2009*, 384-392, San Diego, CA, October 2009.
[58] S.K. Kang, Paul Lauro, Da-Yuan Shih, Donald W. Henderson, Timothy Gosselin, Jay Bartelo, Steve R. Cain, Charles Goldsmith, Karl J. Puttlitz, and Tae-Kyung Hwang, "Evaluation of Thermal Fatigue Life and Failure Mechanisms of Sn-Ag-Cu Solder Joints with Reduced Ag Contents," Proceedings of Electronic Components and Technology Conference, 661, IEEE, Piscataway, NJ (2004).
[59] "High Temperature Package Warpage Measurement Methodology," JEDEC Standard JESD22-B112, JEDEC, Arlington, VA, May 2005, www.jedec.org.
[60] "Reflow Flatness Requirements for Ball Grid Array Packages," JEDEC Standard Procedures and Practices, SPP-024 Issue A, March 2009, JEDEC, Arlington, VA, May 2005, www.jedec.org.